Intensification of photocatalytic hydrogen generation from glycerol under natural sunlight: Cocatalyst effects and solar applicability

Katarzyna Bednarczyk[1]* [ID], Marta Gmurek[2]* [ID]

[1] Lodz University of Technology, Faculty of Process and Environmental Engineering, Department of Safety Engineering, Wolczanska 213, 90-924 Lodz, Poland
[2] Lodz University of Technology, Faculty of Process and Environmental Engineering, Department of Molecular Engineering, Wolczanska 213, 90-924 Lodz, Poland

* Corresponding author, e-mail:
katarzyna.bednarczyk@p.lodz.pl
marta.gmurek@p.lodz.pl

Abstract
This study focuses on intensifying photocatalytic hydrogen generation from glycerol under natural sunlight, examining the effects of cocatalysts and solar applicability. Cocatalysts are commonly employed to enhance the separation of photo-generated charges, while sacrificial agents suppress electron-hole recombination. Utilizing crude glycerol and solar light for photocatalytic hydrogen generation presents a promising avenue. The main objective was to enhance H_2 production from a glycerol-containing solution by selecting parameters and scaling up the process using various reactor types and research systems. The study investigated the applicability of natural sunlight for photocatalytic H_2 production and examined the influence of organic impurities on H_2 production from synthetic and real crude glycerol. Scaling up the process intensified the rate of hydrogen generation, with the highest production achieved using TiO_2 loaded with 0.5% Pt under visible light irradiation. It was concluded that H_2 can be generated by reducing protons from both water and glycerol, the sacrificial agent. Glycerol and water, in the presence of photodeposited Pt or Pd on TiO_2 and light, are converted to H_2 through photocatalytic water-splitting and light-induced oxidation of glycerol. The successful application of photocatalysts under natural sunlight for hydrogen production was confirmed, highlighting the potential for sustainable and scalable green hydrogen generation.

Keywords
hydrogen production, photocatalysis, noble metal modification, water-splitting, cocatalysts

1. INTRODUCTION

Hydrogen is considered an ecological energy carrier with significant potential for reducing greenhouse gas emissions. To evaluate its potential as a fuel source, the overall energy efficiency and viability of various stages need to be considered, including production, purification, transport, storage, and use (combustion) (Dean, 1999; Ibhadon and Fitzpatrick, 2013). An important parameter indicating hydrogen's viability as an energy carrier is its gross calorific value, which is very high (120–142 MJ/kg). This value is more than twice that of methane (50–55 MJ/kg), almost three times that of octane (gasoline) (47.90 MJ/kg), and over five times that of methanol (22.70 MJ/kg). This high calorific value is one of hydrogen's key advantages as a future fuel compared to other energy carriers (Dean, 1999; Bowker et al., 2009).

However, it is crucial to recognize the challenges associated with hydrogen utilization. Due to its very low molar weight, hydrogen requires compression or liquefaction to achieve a usable energy density. This process significantly increases the complexity and cost of hydrogen storage and transportation, particularly for vehicle propulsion. Compressed hydrogen storage necessitates high-pressure tanks, while liquefied hydrogen requires cryogenic temperatures, both of which present technical and economic challenges. Additionally, the energy required for these processes can offset some of the environmental benefits of hydrogen as a clean energy carrier.

The photocatalytic H_2 generation process is performed in the presence of semiconductors that act as photocatalysts. Titanium (IV) oxide is a well-known, non-toxic, and mostly inert photocatalytic material. However, pristine TiO_2 exhibits a low H_2 generation yield, and several methods can be used to improve its visible light absorbance. Modifying the photocatalyst with metal ions is one of the most popular methods. Generally, the modification narrows the bandgap and enhances light absorption, which can be achieved by depositing metals or sensitized dyes that absorb visible light. When TiO_2 is modified with metal nanoparticles (especially noble metals such as Pt, Au, Pd, and Ag), it acts as an electron trapper and can prevent electron-hole recombination. The absorption of radiation of suitable energy (greater than or equal to the bandgap energy, e.g., 3.2 eV for TiO_2 anatase form) excites electrons from the valence band to the conduction band (Bednarczyk et al., 2018; Cybula et al., 2014; Fan et al., 2013;

Fujishima et al., 2000; Fujishima et al., 2007; Rafique et al., 2023; Stelmachowski et al., 2014a; 2014b). Photoexcitation generates highly oxidizing holes and reduces electrons. Catalytic reactions occur at active centers, such as the corners and edges of crystals, contact points between adjacent crystals, and defects in the crystal lattice. The bandgap energy of a semiconductor may reach as much as ~ 2 eV (Bowker et al., 2009). In practice, pristine substances are rarely used as catalysts; the addition of active ingredients via deposition improves the structural and catalytic properties of the material, modifying the bandgap energy. P25-TiO_2 (pristine TiO_2) is an n-type semiconductor, and the n/p transition depends on the type and concentration of the metal deposition (Bednarczyk et al., 2018; Dean, 1999; Ibhadon and Fitzpatrick, 2013).

It is well known that modification of TiO_2-based catalysts/carriers with noble metals increases their activity under visible light, enhances charge transfer, and creates active sites for H_2, significantly increasing H_2 production (Bednarczyk et al., 2018; Daskalaki and Kondarides, 2009; Kumar et al., 2015; Lei et al., 2023; Zaleska, 2008). The effects of many other factors on the efficiency of photocatalytic conversion of organic compounds and water splitting processes have also been widely studied using various catalysts, although most studies focus on noble-metal modification of TiO_2 (Bowker et al., 2009; Daskalaki et al., 2011; Villachica-Llamosas et al., 2024; Zaleska, 2008). One of the most important factors is increasing the spectral sensitivity of TiO_2-based photocatalysts to visible light (Sadanandam et al., 2013; Yu et al., 2010; Yu et al., 2011). The published results are not very optimistic considering the further implementation of the required fabrication methods on a large scale. Maximum hydrogen productivity of 0.22 mmol H_2/h·g_{cat} was observed for water splitting using Cobalt-modified titanium (IV) oxide as a photocatalyst (0.1 g of catalyst suspended in 50 mL of water) under real solar radiation (Gomathisankar et al., 2013). However, our previous study demonstrates that under UV–Vis light, promising high hydrogen production (141 mmol H_2/h· g_{cat}) can be achieved when 0.5 wt.% Pt-modified TiO_2 is used (Bednarczyk et al., 2018).

Replacing current hydrogen production methods requires the development of a cheap, efficient, and fast hydrogen production method. It is important to first consider the total energy balance of all stages of hydrogen production. One of the most promising processes for producing hydrogen is via photocatalytic H_2 generation in the presence of organic compounds (e.g., alcohols and purified glycerol from bio-ester production). Photocatalytic hydrogen (H_2) generation by utilizing crude glycerol and solar light is considered a promising avenue. The present work illustrates enhanced rates of H_2 generation and TiO_2-based catalyst behavior suspended in aqueous synthetic and real crude glycerol solution (industrial byproduct) under visible light irradiation. To the best of our knowledge, for the first time, it was shown that synthetic and industrial byproduct crude glycerol was used as a sacrificial agent to improve photocatalytic efficiency.

This study investigated the applicability of the photocatalytic process for H_2 production from the glycerol–water system under simulated and natural sunlight conditions. Glycerol was selected as a sacrificial agent for improving hydrogen photogeneration. There is a surplus of crude glycerol on the market; it is the main by-product of the transesterification of vegetable oils to produce biodiesel. The increasing amount of crude glycerol may be a serious barrier to the further development of this industry. Photoconversion of glycerol to hydrogen, or bioconversion into hydrogen or other products, may provide a value-added product from a waste product. Therefore, we investigate the mechanism of photocatalytic generation in the presence of crude glycerol as well.

The main goal of this study was to increase the rate of hydrogen generation. Cocatalysts were applied to improve the separation of photogenerated charges, facilitating the water oxidation or reduction reaction. To substantially suppress electron-hole recombination and increase the rate of hydrogen generation, a sacrificial agent was added. The objective of this paper is to present a strategy for photocatalytic H2 generation using different types of reactors. To achieve this, we combine a detailed analysis of experimental conditions such as the light source, photoreactor, amount of catalyst, type of catalysts with different cocatalysts loading, amount and type of sacrificial reagent, configuration of lamp and photoreactor, etc. Moreover, to reinvigorate industrial interest in the technology, tests on real crude glycerol have been done. Therefore, the study aimed to investigate: (1) production of H_2 from a glycerol-containing solution, selections of process parameters, and increasing the scale of the process through the use of various types of reactors and research systems; (2) applicability of natural sunlight for photocatalytic production of H_2; and (3) the influence of organic impurities on H_2 production from synthetic and real crude glycerol.

2. MATERIALS AND METHODS

2.1. Materials

All reagents used in this work were analytical grade and were used without further purification. Glycerol (GLC; $\geqslant$99%) and 4 hydroxybenzoic acid methyl ester were purchased from Sigma-Aldrich. Methanol (MeOH; > 99%) and 96% ethanol (EtOH) was purchased from Stanlab and ChemLand, respectively. 1–butanol (1-BuOH; > 99%) and 1–propanol (1-PrOH; > 99%) were purchased from Chempur. All solutions were prepared using deionized (DI) water from a Millipore system (Direct-Q®, Merck Millipore). Argon gas (purity > 99%) was purchased from Air Products.

2.2. Catalyst preparation

All photocatalysts were obtained by UV reduction of Pt^{4+} or Pd^{2+} ions in a TiO_2 suspension. An aqueous solution of alcohol (ethanol and isopropanol, 99.8%; Polchem) was used

as a hole scavenger and contained TiO_2 microspheres (3 g) and metal precursor (0.1, 0.5, or 1% wt. Pt or Pd). This solution was sonicated for 10 min, stirred in the dark for 2 h, degassed with nitrogen in the dark for 1 h, and finally illuminated using a 1000-W Xe lamp (Osram) as an irradiation source. Details of this procedure are as follows. An aqueous solution of isopropanol containing H_2PtCl_6 (99%; Sigma Aldrich) or $PdCl_2$ (5 wt.% solutions in 10 wt.% HCl; Sigma Aldrich) was degassed with nitrogen and irradiated using UV–Vis light from a 1000 W Xe lamp) for 6 h. The modified TiO_2 photocatalysts were rinsed with DI water, separated by centrifugation, and then dried at 65–120 °C for 12 h without calcination. The temperatures used to dry the catalysts did not modify their properties and only removed humidity from the pores. To achieve Pd doping at concentrations of 0.1 wt.%, 0.5 wt.%, and 1 wt.%, the precursor concentrations of $PdCl_2$ were 4.02×10^4 mol/L, 2.01×10^3 mol/L, and 4.02×10^3 mol/L, respectively. Similarly, the precursor concentrations of H_2PtCl_6 for Pt-doped catalysts were 2.2×10^4 mol/L, 1.1×10^3 mol/L, and 2.2×10^3 mol/L for 0.1 wt.%, 0.5 wt.%, and 1 wt.%, respectively.

2.3. Catalyst characterization

The optoelectronic properties of the pristine TiO_2 and modified catalysts were evaluated by performing diffuse reflectance spectroscopy measurements (DRS–UV/Vis) in the region of 250–700 nm using an Evolution 220 spectrophotometer (Thermo Scientific, Waltham, MA, USA) applying $BaSO_4$ as the internal reflectance standard. Spectra were recorded in diffuse reflectance mode and transformed to a magnitude proportional to the extinction coefficient (α) employing the Kubelka–Munk function $(F(R_\infty))$ where R_∞ represents the relative percentage of reflectance of the catalyst sample with respect to the reference. The optical band gaps were analyzed using converted Tauc plot by the Kubelka–Munk method and with the application of baseline in the sub-bandgap region approach (based on formula indirect transitions gap) according to Equation (1) based on (Makula et al., 2018).

$$(F(R_\infty) \cdot h\nu)^{\frac{1}{\gamma}} = B(h\nu - E_g) \tag{1}$$

Where B is a constant, $h\nu$ is the photon energy, and E_g is the bandgap. The γ factor depends on the nature of the electron transition therefore direct and indirect transition band gaps can be calculated when γ is equal to 1/2 or 2, respectively (Makula et al., 2018).

Details about characterization techniques methodology: BET, SEM, XRD, and XPS can be found in our previous papers (Bednarczyk et al., 2018; Borowska et al., 2019; Gomes et al., 2017; Gmurek et al., 2019).

2.4. Catalytic activity for hydrogen production

2.4.1. Preliminary study

The experiments were carried out on a "merry-go-round" device with quartz tubes placed between two exposure panels (Luzchem). Each panel consisted of four low-pressure mercury lamps (USHIO, model G8T5 Hg (7.2 W each)) with a maximum emission of 254 nm. The photon flux rate is equal to 1.56×10^{-4} Einstein/m^2 s was previously determined using uranyl oxalate and confirmed by measuring with a radiometer (UV–Vis–NIR, Ocean Optics USB4000, USA). The volume of the quartz tube was equal to 13 mL, with an average optical path length of 0.85 cm. Each quartz tube was occupied by a septa and a small hydrogen storage balloon (Fig. 1A). Additionally, the next panel with XBO lamps was used. H_2 was generated and stored continuously for 2 h. After experiments, H_2 was sampled and injected (50 μL) for analysis.

2.4.2. Artificial light

Photocatalytic reaction experiments were performed in a glass semi-batch reactor (1200 mL, Fig. 1C) with a quartz immersion cooling well where the light source was placed. Additionally, the reactor was occupied with a cooling jacket and the temperature was stable at 25 ± 5 °C. The volume of the reaction solution containing the aqueous glycerol solution and photocatalysts was 600 mL. A 100-W Xe arc lamp was used to simulate sunlight and was placed on the vertical axis of the reactor. At the start of each test, the reactor was loaded with an aqueous glycerol solution (4.5 wt.%) and/or other alcohols such as methanol (MeOH), ethanol (EtOH), 1–propanol (1–PrOH), and 1–butanol (1–BuOH), to which the photocatalyst was then added. Suspension of the catalyst in the reaction mixture was obtained by magnetic stirring. Argon was used as a carrier gas in all tests with a flow rate of 150 mL/min. The flux of argon removed gases from the solution, such as dissolved oxygen, as well as oxygen, hydrogen, and carbon dioxide produced during the photocatalytic process (this stream of gaseous products was then analyzed by GC). Carbon dioxide concentration measurements were made using an LB-854 meter (LAB-EL), which was located in the discharge gas loop into the GC system. Each experiment lasted approximately 4 to 6 h.

2.4.3. Natural sunlight

For this purpose, a specially designed reactor was applied. The reactor was made of boron glass with a special quartz glass upper layer. The total capacity of the reactor was 500 mL with a working volume of 250 mL (Fig. 1D). The bottom of the reactor was equipped with a bubble system responsible for distributing the carrier gas and mixing the solution. During the process, measurements of oxygen concentration, carbon
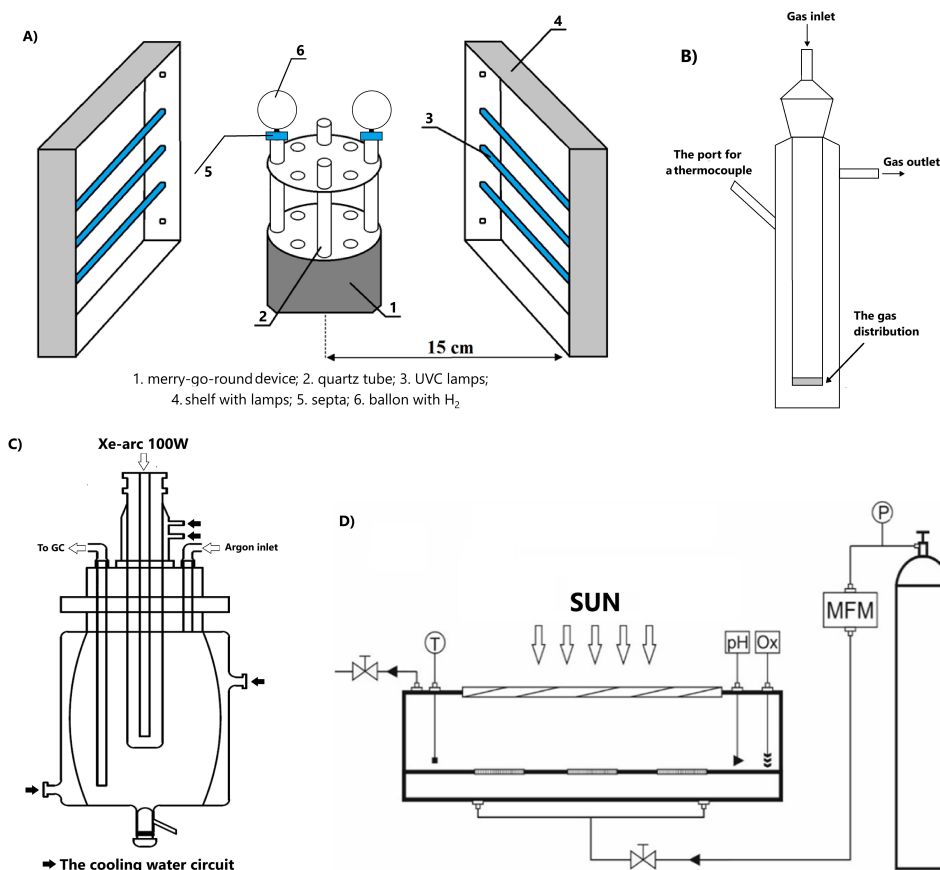
Figure 1. Schematic diagrams of the (A) rector for preliminary study; (B) small-lab reactor (40 mL) for H_2 production from synthetic and real crude glycerol solution; (C) large reactor (1200 mL) with the cooling water circuit, (D) reactor for experiments in the Sun (500 mL).

dioxide, pH, and reaction temperature were performed. Additionally, the same setup was used for comparison with artificial XBO 100 W and 150 W. At the beginning of the process, the reaction temperature was 25 °C, which increased to 40-55 °C during the experiments, depending on the weather conditions.

2.4.4. Photocatalytic H_2 generation from synthetic and real crude glycerol solution

The photocatalytic generation of H_2 from the synthetic and real crude glycerol solution was performed in a semi-batch quartz reactor with a volume of 40 mL (Fig. 1B). The volume of the reaction solution containing a mixture of water, the selected organic ester (4-hydroxybenzoic acid methyl ester), and the photocatalyst was 16 mL. Three external xenon lamps (Xe-arc XBO; 75 W each) were used to simulate sunlight. The reactor was loaded with an aqueous solution containing glycerol (1.5 wt.%), methanol (1 wt.%), rapeseed oil (2 wt.%), 4-hydroxybenzoic acid methyl ester (0.1% wt.%) (MP, methylparaben), and 0.083 g/L of 1 wt.% Pt/TiO$_2$. During the experiments, the temperature was measured but not controlled. At the start of the process, the reaction temperature was 25 °C, which increased to 55 °C during the experiments. Argon with a flow rate of 30 mL/min was used as a carrier gas in all tests to remove dissolved oxygen (before the start of each run) and

remove gaseous products from the reaction mixture during the experiment. Suspension of the catalyst in the reaction mixture was obtained by magnetic stirring and bubbling argon.

2.5. Analytical methods

A gas chromatograph (Perkin Elmer) equipped with a TCD detector was used for the analysis of the gas phase. The volume of the gas sample was 1 mL. The evolved gases were analyzed every 15 min using a silica gel-packed column (Altech 5651 PC). The chromatographic conditions were as follows: injector port temperature of 200 °C, detector temperature of 220 °C, a temperature program of 120 °C for 3.5 min, ramp up to 180 °C at 40 °C/min, and then held for 4 min.

Samples were taken from the liquid phase after the reaction was complete and analyzed using a gas chromatography/mass spectrometry system equipped with a headspace Shimadzu Ultra GCMS-QP2010. A gas chromatograph with a mass detector enables the analysis of organic compounds in both the gas and liquid phases. The mass range of the analyzed compounds: m/z was 1.5–1090. The chromatographic conditions were as follows: column temperature of 40 °C, injection temperature of 260 °C, pressure of 15.5 kPa, and column flow of 1.56 mL/min.

Carbon dioxide concentration measurements were performed using a LAB-EL LB-854 meter based on the non-dispersive infra-red (NDIR) detector method, which is now the industry standard for measuring the concentration of carbon oxides (CO and CO_2). This technique is based on the measurement of the attenuation of IR radiation at a specific wavelength transmitted by the measured gas, where its suppression is dependent on the carbon content in the test gas. The NDIR method provides accurate and stable measurement results. A sensor for measuring CO_2 was placed inside the controller and fed with the gas stream to be analyzed, which allowed the gas to be supplied from a distant source. The measurement range of the volume content of CO_2 was 0–10000 ppm (0–1%), while the accuracy of CO_2 measurement at $22\,°C$ was $\pm5\%$ of the measured value plus ±100 ppm.

3. RESULTS AND DISCUSSION

3.1. Preliminary study – enhancement by visible light

A preliminary study focused on investigating the improvement of hydrogen generation under different light irradiations. Therefore, experiments have been conducted with the application of a monochromatic UVC lamp (254 nm; 44.4 W/m^2 equals 1.56×10^{-5} Einstein/m^{2}s) as well as a polychromatic Xenon arc lamp ($\lambda > 370$ nm; 192.02 W/m^2 equals 6.76×10^{-4} Einstein/m^{2}s) used as artificial sunlight. The experiments were performed on a "merry-go-round" device with quartz tubes, each occupied by a septa and a small hydrogen storage balloon (more details in the Methods section). 13 mL of the aqueous solution of glycerol (4.5 wt.%) in the presence of 70 mg (5.38 g/L) catalyst modified by 0.1wt% of Pt, Pd, Ag, and Au. Additionally, as a baseline, pristine TiO_2 has been applied. Fig. 2 presents cumulative hydrogen after 1 hour of irradiation. As can be seen, H_2 generation is enhanced under visible light. Modification by noble metals favors photocatalytic production compared to pristine TiO_2 (1.18 mmol of H_2 and 0.02 mmol of H_2 under visible and UVC light, respectively). Apparent quantum yield (AQY) calculation (twice the ratio of the number of produced hydrogen molecules to the number of incident photons) is often used for photocatalytic activity description. For evaluation of photocatalytic activity following AQY was determined for the primary experiments with 0.1 wt.% modification as well as for 1 wt.% of Platinum TiO_2 modification for 4.5% glycerol solution.

The highest H_2 efficiency has been observed for Pt_TiO_2 catalysts for both light sources (273.46 ± 3.17 mmol of H_2 (Vis, AQY equals 14.3% for 420 nm) and 25.97 ± 0.15 mmol of H_2 for (UVC, AQY equals 9.7). Interestingly, considering Pd_TiO_2, slightly lower H_2 efficiency was observed under UVC light (24.44 ± 0.49 mmol of H_2) compared to Pt_TiO_2. While, when XBO lamps have been used the efficiency of Pd_TiO_2 was much lower and comparable to Ag_TiO_2 (219.46 ± 0.42 and 209.17 ± 0.85 mmol of H_2, respectively). Au_TiO_2 seems to be the worst catalyst under visible and UVC light.

Modifying TiO_2 by a metal enables visible-light-activated photocatalysis and enhanced hydrogen generation efficiency by improving the separation of photo-generated charges (the Schottky barrier formation at the metal-semiconductor interface). It is known that the Fermi level of unmodified TiO_2 is higher than that of noble metals; therefore, modification results in the effective transfer of the photogenerated electrons from the conduction band of TiO_2 to the metal particles. On the basis of that electron trapping process, the electron-hole recombination rate is significantly reduced, causing stronger photocatalytic reactions. Therefore, the enhancement of photoactivity in the visible range arises from the prolongation of the lifetime of charge carriers. As mentioned, the noble metal acts as an electron trap, and the transfer of electrons from TiO_2 to substrates is accelerated (Grabowska et al., 2018; Janczarek and Kowalska, 2017). These photocatalysts have also used plasmonic properties to gain activity under visible-light irradiation (Grabowska et al., 2018; Janczarek and Kowalska, 2017; Zaleska, 2008). As can be concluded, an improvement in photocatalytic activity and H_2 generation efficiency can be observed due to minimizing electron-hole recombination that is enabled by the cocatalytic role of Pt and Pd. Given that Pt has a higher work function (5.65 eV) than Pd (5.12 eV), this resulted in a higher Schottky barrier (the lower Fermi level) that inhibits the recombination of photogenerated charges. However, according to the volcano plot of hydrogen evolution in metal catalysts, the hydrogen evolution reaction (HER) in Au is limited by its lower binding energy (metal–hydrogen bond) compared to Ag, Pd, and Pt (Greeley et al., 2006).

The visible-light activities originate from the changes in the band-gap structure of the semiconductor resulting from noble metal modification. The optical properties of the photocatalysts obtained by the photodeposition method (Pd_TiO_2, Pt_TiO_2, and Ag_TiO_2) and the sol-gel (Au_TiO_2) were investigated by diffuse reflection spectroscopy. Fig. 3 shows the UV/Vis DRS spectra for TiO_2 photocatalysts modified by 0.1 wt.% (A) and 0.1 wt.%, 0.5 wt.%, and 1 wt.% modification of Pd and Pt (B, C).
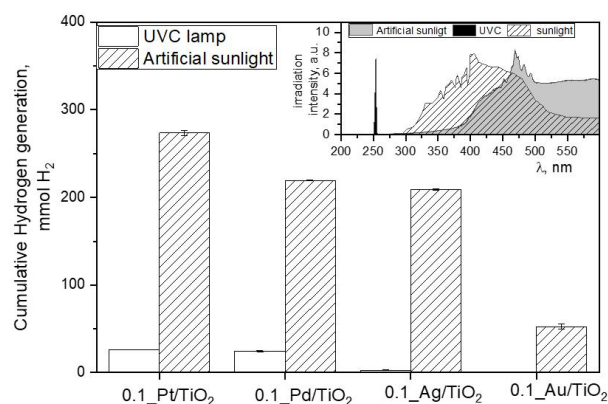
Figure 2. Cumulative hydrogen generation after UVC and Visible light irradiation in the presence of modified catalysts. Insert: Emission spectra of different light sources (UVC, XBO, and sunlight).

The spectrum of unmodified TiO_2 clearly shows an absorption onset at about 400 nm while above 400nm P25-TiO_2 (pristine TiO_2) does not exhibit any absorption ability. Conversely, visible light absorption enhancement has been clearly shown after modification (significant for Pt and Pd loaded catalysts). As can be seen in Fig. 3A, modification by 0.1wt.% is the most sufficient for Pt_TiO_2, which confirms preliminary results. Moreover, spectra of Pt_TiO_2 and Pd_TiO_2 overlap in the UV region, which can explain similar H_2 efficiency of those catalysts under UVC light. Surprisingly, the spectra for Pd_TiO_2 and Ag_TiO_2 confirm similar visible light absorption ability, which was shown in the similar H_2 efficiency for the XBO lamp. When different loadings are considered, the highest absorption of light in the visible range is shown by the 1_Pt/TiO_2 photocatalyst containing 1 wt. % of platinum. A bathochromic shift of the absorption maximum was also observed for palladium-modified photocatalysts. Undoubtedly, there is a trend of improvement in visible light absorption with increasing metal content (for Pd and Pt) when the photodeposition method is considered. In the case of the sol-gel synthesis method, the highest absorption in the visible light range is shown by the 1_Pd/TiO_2 photocatalyst containing 1 wt. % palladium. However, in the case of platinum modification by the sol-gel method no differences can be observed for samples with a content of 0.5 wt. % and 0.1 wt. % (0.5_Pt/TiO_2 and 0.1_Pt/TiO_2, respectively).

Several characterization techniques, including BET, SEM, XRD, and XPS, have been used for morphological and surface characterization of catalyst samples and discussed in our previous papers (Bednarczyk et al., 2018; Borowska et al., 2019; Gomes et al., 2017; Gmurek et al., 2019). Chemical composition of the noble metal decorated TiO_2 obtained from XPS measurement of various modification loadings are provided in Table 1. In almost all cases the lowest loadings were below detection, only modification with Pt confirmed its presence in the structure (atomic Pt content equal to 0.08%). For silver and gold modification (0.1 wt.%), it was not possible to precisely measure the contents (data not shown).

However, for 0.5_Ag/TiO_2 0.47 atom% was successfully deposited on the TiO_2 surface, while for 0.5_Au/TiO_2 only 0.02 atom% of Au was detected. As discussed by Borowska et al. (2019), XPS measurements of catalyst with higher leadings (0.5 wt.% and 1 wt.%) the analyzed content of deposited metals are lower than assumed due to lower yield of the photodeposition method. But still, the highest atomic content was detected for highest loading, 0.61 atom% and 0.70 atm% for 1_Pt/TiO_2 and 1_Pd/TiO_2, respectively (Table 1). This finding has been confirmed by SEM analysis, that can be found in (Borowska et al., 2019). The high-resolution XPS spectra for Pd3d and Pt4f and XPS survey spectra are depicted and discussed in (Borowska et al., 2019). The surface area of P25-TiO_2 (pristine TiO_2) was shown to be 50 m^2/g. For catalysts prepared by photodeposition decolored by Pt and Pd nanoparticles method BET surface area equaled 55 m^2/g (for highest leadings) and 53 m^2/g for 0.5 wt.% (Borowska et al., 2019). The highest BET surface area of ~ 135 m^2/g was analyzed for catalyst modified by sol-gel method with Au nanoparticles. X-ray diffraction (XRD) analysis showed that phase concentrations did not depend on the amount of metal modification, and the original 80% anatase and 20% rutile fraction were mostly maintained (Bednarczyk et al., 2018). With increasing Pt concentration, the crystallite size increased from 19.6 nm to 22.0 nm for anatase and decreased from 41.5 nm to 21.6 nm for rutile.

The corresponding bandgaps (E_g) were determined from the Tauc plot of the transformed Kubelka–Munk function as it results from the estimation presented in Table 1. The bandgap results confirmed that with increasing load of nanoparticles, the bandgap decreased. For catalysts prepared by photodeposition and for sol-gel method, the lowest E_g were found to have Pt/TiO_2 compared to Pd/TiO_2. The bandgap value for the photocatalysts obtained by the photodeposition method was lower than that obtained by the sol-gel method (data not shown). Pt and Pd modified TiO_2 by the photodeposition method have been selected for further investigation based on characteristic results and E_g.
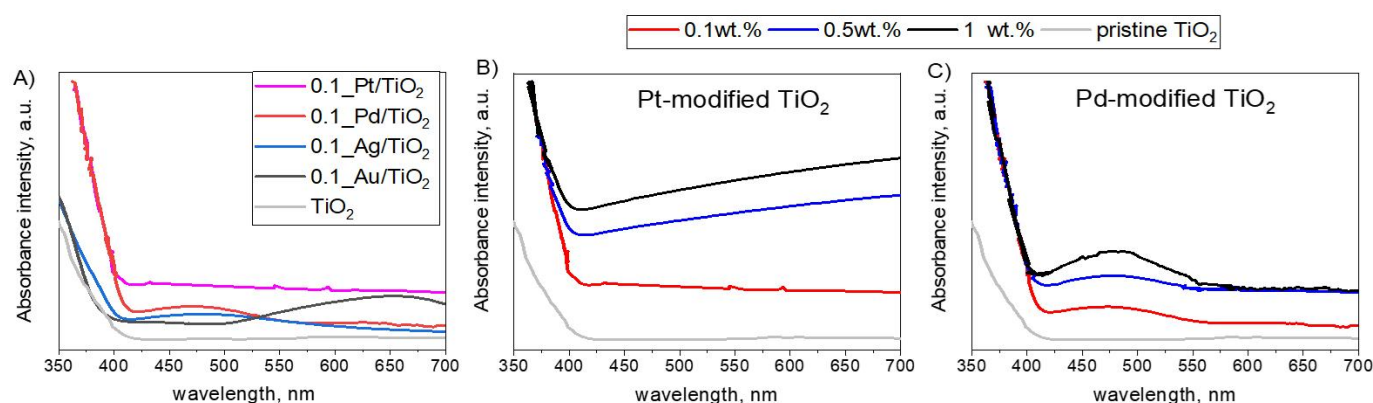
Figure 3. UV/Vis DRS spectra of TiO_2 photocatalysts modified with 0.1 wt.% loading of Pt, Pd, Ag and Au (A) as well as of TiO_2 catalysts with Pt and Pd loadings from 0.1 to 1 wt% (B and C, respectively).

Table 1. Characterization of photocatalysts: determined bandgap, XRD analysis, specific surface area (BET), relative elemental metal concentrations obtained from XPS analysis (characteristics summarized based on our previous research (Bednarczyk et al., 2018; Borowska et al., 2019; Gomes et al., 2017; Gmurek et al., 2019)).

Catalysts	E_g [eV]	Anatase [%]	Rutile [%]	Crystallite size [nm]	BET [m^2/g]	O Content [at.%]	Ti Content [at.%]	C content [at.%]	Metal content [at.%]
0.1_Pt/TiO$_2$	3.054	80	20	18.4–19.6	54	48.57±0.43	21.11±0.17	30.25±0.59	0.08±0.01
0.5_Pt/TiO$_2$	3.031	79	21	19.8–21.5	53	48.70±0.55	20.73±0.01	30.46±0.54	0.13±0.01
1_Pt/TiO$_2$	3.017	80	20	20.0–22.0	55	46.74±0.27	18.13±0.04	34.23±0.13	0.61±0.01
0.5_Pd/TiO$_2$	3.051	80	20	20.3–22.3	53	55.88±0.05	23.66±0.62	20.24±0.66	0.23±0.01
1_Pd/TiO$_2$	3.033	88	12	19.1–20.6	55	54.95±0.41	23.40±0.32	20.95±0.05	0.70±0.02
0.5_TiO$_2$-Au*	–	99	1	10–12	135	14.30±0.07	76.20±0.44	9.48±0.37	0.02±0.00
0.5_TiO$_2$-Ag	–	80	20	45–52	34	58.63±0.66	23.84±0.25	17.06±0.88	0.47±0.04

BET for P25-TiO$_2$ (pristine TiO$_2$) = 51 m^2/g; TIP= 160 m^2/g; E.g. for 0.1_Pd/TiO$_2$ equals 3.066 and for P25-TiO$_2$ (pristine TiO$_2$) equals 3.297; *– prepared by sol-gel method calcined in 400 °C

3.2. Up-scale artificial sunlight experiments

The first part of this study involved the selection of parameters for different types of reactors. This was done from several perspectives to maximize hydrogen production, including the type of catalyst, catalyst dose, and type of organic compound dissolved in the water. The glycerol concentration was the same for all runs (4.5 wt.%). The influence of the type and concentration of metal loading was determined. An important aspect of the research was the intensification of process parameters and the scaling up of the process using various types of reactors and research systems. The process was upgraded from a 40 mL to a 1200 mL reactor (working solution 16 mL and 600 mL, respectively). Based on our previous research, where experiments were performed in the small reactor (40 mL) we assumed that water splitting and glycerol conversion into hydrogen occurred simultaneously. The highest H$_2$ production was obtained for the aqueous solution of glycerol (4.5 wt%), for Pt_TiO$_2$ (0.5 wt.% of Pt, prepared by the photodeposition method and calcined). The average H$_2$ generation efficiency was 137.53 ± 4.31) mmol H$_2$/h·g$_{cat}$ (while the maximum yield reached during the experiments was 141.84 mmol H$_2$/h·g$_{cat}$). To investigate the scaling-up effect, the concentration of the catalyst was kept at 0.083 g/L, as in the smaller reactor. As shown in Fig. 4A, scaling up improved H$_2$ production. When P25-TiO$_2$ (pristine TiO$_2$) was applied, the efficiency of H$_2$ generation reached $\sim$ 5.6 mmol H$_2$/h·g$_{cat}$ in the scaled-up system, while in the small reactor, it was by half lower. Modified TiO$_2$ with photodeposited Pt and Pd significantly increased productivity. Moreover, the Pt-modified

catalysts achieved higher hydrogen production efficiency than Pd-based catalysts. However, it should be noted that the smaller reactor worked with an external light source, while the larger reactor with an internal light source. Therefore, the next intensification and scaling up were performed using the same experimental equipment.

Based on preliminary results, Pt/TiO$_2$ and Pd/TiO$_2$ were selected. The increase in metal loadings had a positive impact on visible light ability, making it reasonable to investigate this parameter. As shown in Fig. 3A insert, the H$_2$ evolution rate slightly depended on noble metal loading. For three loading levels of Pt nanoparticles, we obtained 150.0 ± 1.75 mmol H$_2$/h·g$_{cat}$, 161.48 ± 2.10 mmol H$_2$/h·g$_{cat}$, and 147.51 ± 1.15 mmol H$_2$/h·g$_{cat}$ for 0.1, 0.5, and 1 wt.% loadings, respectively. For Pd/TiO$_2$ catalysts, the H$_2$ evolution rate was found to be almost equal across all Pd loadings (0.1 wt.% –118.92 ± 1.94 mmol H$_2$/h·g$_{cat}$, 0.5 wt.% – 125.52 ± 1.57 mmol H$_2$/h·g$_{cat}$, 1 wt.% –120.54 ± 1.43 mmol H$_2$/h·g$_{cat}$). In both cases, insignificantly higher values were found for 0.5 wt.% loadings.

High H$_2$ productivity is the obvious goal for reaction engineering and reactor design. The H$_2$ evolution is strongly dependent on the catalyst used. Thus, the catalyst selection and its applied dose play a vital role in the success of scaling-up of this process. Therefore, a next step of investigation was to examine the influence of catalyst dose (0.015 g–0.58 g per 600 mL, 100 W internal light 3.16 × 10^{-6} Einstein/m^{2}s)). As mentioned above, the productivity of H$_2$ is commonly described by the rate of H$_2$ evolution (mmol H$_2$/h·g$_{cat}$). But

when the catalyst dose is examined, this unit could lead to misunderstanding (due to the calculation per catalyst dose). Here, the evolution of H_2 is presented as an amount of produced H_2 in mmol. The highest hydrogen evolution after 2 h was achieved for the highest catalyst dose – 9.67 ± 0.09 mmol of H_2 (Fig. 4). However, considering the cost of catalysts, the best solution has to be obtained. Based on this approach, the concentration of 0.05 g per 600 mL (0.083 g/L) could be considered an efficient one. When 0.05 g was applied (more than 10 times lower than the highest dose), the H_2 concentration was less than twice lower (5.41 mmol of H_2 compared to 9.67 mmol of H_2). It should be noted that when the lowest catalyst dose was used, 3.40 ± 0.07 mmol of H_2 was produced in a solution containing 4.5 wt.% GLC, while without glycerol, 1.37 ± 0.07 mmol of H_2 was generated. The irradiation of solution without GLC and catalyst was not able to produce hydrogen. Upscaling to 800 mL with the application of a more powerful lamp led to significant improvement (Fig. 4: Insert).
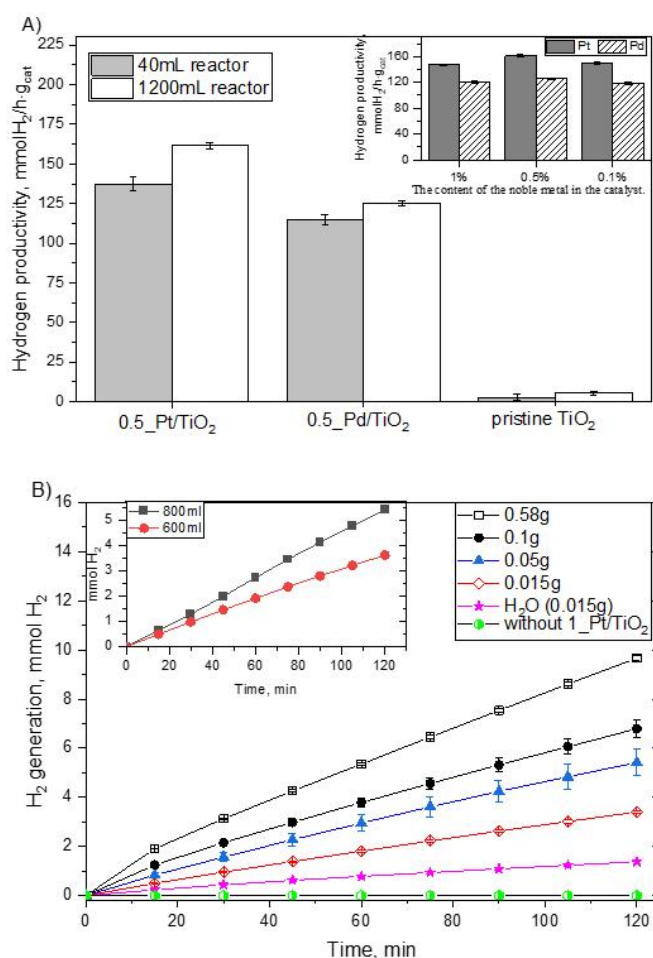
Figure 4. A) Effect of upscaling for Pt and Pd modified catalysts loaded by 0.5 wt.%, Insert: Catalyst type and content of metal modification influence on H_2 generation (4.5% wt. GLC, 100 W; 0.083 g/L of catalyst). B) Catalyst dose influence on H_2 generation (1_Pt/TiO$_2$, 4.5% wt. GLC, 100 W). Insert: Increasing the reactor volume from 600mL to 800mL (1_Pt/TiO$_2$, 4.5% wt. GLC, 150 W for 800 mL and 100 W for 600 mL, 0.03 g/L).

Different organic substances (e.g., alcohols, oils, and sugars) influence hydrogen yield when dissolved in reaction water (Chen et al., 2018; Chen et al., 2020; Gomathisankar et al., 2013; Gombac et al., 2010; Hainer et al., 2018; Jovic et al., 2013; Kumar et al., 2016; Villachica-Llamosas et al., 2024). The addition of sacrificial hole scavengers such as methanol is a commonly used practice in semiconductor photocatalysis to promote electron-hole pair separation after photoexcitation (Daskalaki and Kondarides, 2009; Daskalaki et al., 2011; Gombac et al., 2010; Kumar et al., 2016). The addition of an alcohol sacrificial agent (sacrificial electron donors) quenches electron-hole pair recombination in the semiconductor (progressively oxidized by valence band holes on the photocatalyst surface), thus accelerating the H_2 production efficiency of metal-modified TiO$_2$ photocatalysts under visible and UV excitation (Chen et al., 2018; [5]Chen et al., 2020; Gombac et al., 2010; Hainer et al., 2018; Kumar et al., 2016).

Investigating the impact of glycerol on the productivity of H_2 in the small reactor confirmed this hypothesis (Fig. 5). The highest yield – 55.82 mmol/h·g$_{cat}$ was obtained for 4.5% glycerol with the addition of a metal-loaded photocatalyst. However, for the addition of pristine TiO$_2$, the hydrogen production was 86% lower than for the platinum-modified photocatalyst. For water with a 0.5 wt. % Pt/TiO$_2$ photocatalyst, the yield was 33% lower than for the glycerol solution, while for water with the addition of pristine TiO$_2$, no hydrogen peak was obtained. Interestingly, when Pt/TiO$_2$ was applied with a load of 0.5 wt.%, an acceleration in H_2 productivity was observed even after 0.5% glycerol addition compared to water. While when pristine TiO$_2$ was used, H_2 was generated only in the presence of 4.5 % glycerol. In a bigger reactor, as shown in Fig. 4A, experiments performed with P25-TiO$_2$ (pristine TiO$_2$) suspended in a water-glycerol solution showed very low hydrogen production (5.62 mmol H$_2$/(h· g$_{cat}$)).
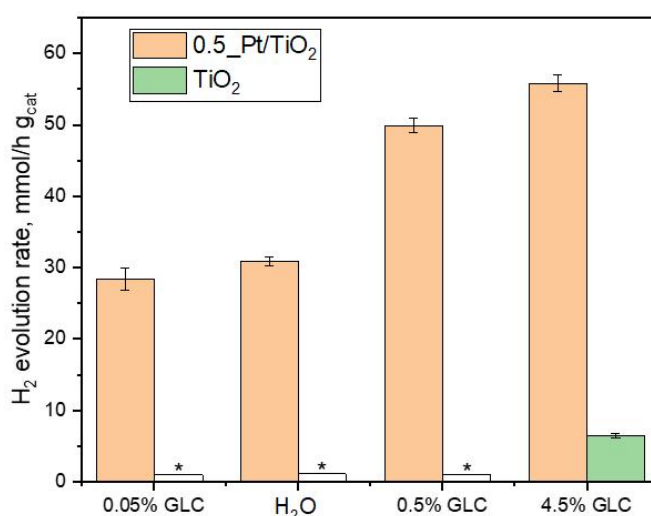
Figure 5. Effect of glycerol addition on H_2 generation in the presence of Pt/TiO$_2$ catalyst loaded by 0.5 wt.% and pristine TiO$_2$ (40 mL reactor, 225 W (3 lamps); 0.93 g/L of catalyst).

No H_2 was detected when pristine TiO_2 was applied to water or when the experiment was carried out without catalysts (Table 2). Moreover, for the reaction without irradiation, the efficiency of hydrogen production was also negligible. However, experiments using modified TiO_2 by noble metals in water showed a H_2 productivity of ~ 13 mmol $H_2/(h \cdot g_{cat})$. Unmodified TiO_2 is known to be inefficient for H_2 generation as a result of rapid electron-hole recombination, leading to the limitation of charge carriers available for photoreactions (Jovic et al., 2013). Table 2 shows the hydrogen yields when different alcohols, such as glycerol (GLC), methanol (MeOH), ethanol (EtOH), 1–propanol (1-PrOH) and 1–butanol (1-BuOH) were added to the water. The following trend was observed: GLC > MeOH > EtOH > 1-PrOH > 1-BuOH > pure water. This finding is in agreement with our previous results on a smaller scale (Bednarczyk et al., 2018). As can be seen, true water splitting in the absence of sacrificial donors (that act as hole traps) is very inefficient even when Pt_TiO$_2$ is considered. The H_2 production from pure water is around 10% of the overall H_2 production when GLC is presented.

The study examined the influence of glycerol concentration on H_2 yield. Optimal hydrogen production occurred with glycerol concentrations between 1% and 12% (Fig. 6), with the highest rate observed at 9% glycerol concentration. The cumulative production of H_2 after 2 h is shown in Fig. 6 inset; these data also did not show a clear trend. Only slightly higher H_2 concentration was detected when using higher glycerol contents. Yet these differences were not significant. Therefore, the optimal concentration of glycerol cannot be predicted with sufficient precision. This may be because the photoconversion of glycerol into hydrogen and water splitting occurred simultaneously, making it difficult to separate these processes. If the presence of glycerol in water influences the rate and yield of the water-splitting reaction, it is very difficult to determine the effect of the concentration of glycerol on the total hydrogen production. Hence, further studies are required.

3.3. Natural sunlight experiments

In small-scale experiments, the effect of lamp power – radiation intensity on the efficiency of H_2 production was determined (Bednarczyk et al., 2018). As expected increasing photon entry to the solution resulted in higher H_2 efficiency. While the natural sunlight experiments were planned, a preliminary study with a new reactor for experiments in the sun was
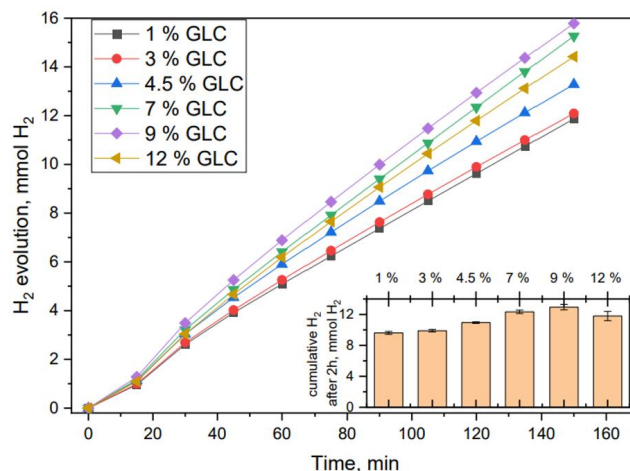
Figure 6. Influence of glycerol concentration on the hydrogen productivity over time with a catalyst concentration of 0.083 g/L and 1 wt.% Pt/TiO$_2$ catalyst.

performed. The difference was in the construction of the reactor and in the irradiation of the reaction mixture system by an external light source. The mixture was a solution of 250 mL of 4.5 wt.%. GLC with the addition of a TiO_2 photocatalyst with the deposition of Pt or Pd metal and irradiation of the system with a xenon lamp: with a power of 100 W and 150 W. Then, for the same conditions, the photocatalytic production of H_2 was carried out using solar radiation (in August 2017 – experiments were performed between 10 a.m. and 2 p.m.). As can be seen in Fig. 1 insert, the emission spectrum of natural sunlight contains UVA and visible light (from 300 nm), while the XBO lamp emits radiation above 370 nm.

The influence of the radiation intensity is confirmed by the use of different lamp powers for this reactor: 100 W and 150 W. For the 0.5_Pt/TiO$_2$ photocatalyst and the 150 W lamp, the efficiency of H_2 production was 28.53 mmol $H_2/(h \cdot g_{cat})$, while for 100 W – 25.17 mmol $H_2/(h \cdot g_{cat})$.

Photocatalysis is one of the main approaches to producing hydrogen by utilizing solar energy. A summary of the photocatalysts and the main results is reported in Table 3. The results showed the influence of the type and power of radiation on the efficiency of H_2 production. It was found that under natural sunlight, higher radiation intensity resulted in higher H_2 productivity. The highest efficiency of H_2 production was obtained for the photocatalysts modified with Pt and Pd with 0.1 wt.% and 0.5 wt.%., respectively. For 0.5_Pt/TiO$_2$, the highest

Table 2. Influence of sacrificial electron donor additives (4.5 wt.%) on H_2 production. The concentration of the catalyst was 0.083 g/L and 1 wt.% Pt_TiO$_2$ catalyst was used

The type of solvent	GLC $C_3H_8O_3$	MeOH CH_4O	EtOH C_2H_6O	1-PrOH C_3H_8O	1-BuOH $C_4H_{10}O$	Water H_2O	WATER H_2O*
Average hydrogen yield, mmol $H_2/(h \cdot g_{cat})$	147.52±1.45	124.24±2.34	98.65±1.89	72.54±1.45	56.31±1.97	13.56±1.68	0

* H_2 was not detected in two experiments (1) without the addition of a photocatalyst and (2) with pristine TiO_2

Table 3. Photocatalytic H_2 yield under natural sunlight (4.5 wt.% GLC, photocatalyst: 0.083 g/L, Pt/TiO_2 and Pd/TiO_2 with different loading)

Type of photocatalyst	1_Pt/TiO₂	0.5_Pt/TiO₂	0.1_Pt/TiO₂	1_Pd/TiO₂	0.5_Pd/TiO₂	0.1_Pd/TiO₂
The average yield of H_2 production, mmol $H_2/(h \cdot g_{cat})$	30.1	47.02	45.58	28.26	41.97	41.05
The highest productivity of H_2, mmol $H_2/(h \cdot g_{cat})$	35.45	66.34	58.46	31.21	45.56	43.14
The highest concentration of H_2, ppm	0.232	0.435	0.383	0.205	0.299	0.283
Average CO_2 concentration, ppm	21	24	23	21	22	22
Average the concentration O_2 in solution, ppm	0.87	1.75	1.69	1.26	1.43	1.49
Average irradiance, W/m²	305.2	337.3	320.6	310.1	312.4	315.4

production efficiency was 66.34 mmol $H_2/(h \cdot g_{cat})$ at irradiance greater than 450 W/m². The measured concentration of CO_2 and O_2 in the solution increased with increasing H_2 production efficiency. The pH of the solution for 0.5_Pt/TiO₂ decreased from the value of 5.27 to 3.25, which is the result of dissolving a part of the CO_2 in the solution. For these process conditions, the decomposition of GLC was small (around 1%).

The reactor platform was adjusted to allow maximum illumination to sunlight and to check the activity of photocatalysts in the photocatalytic reaction of H_2 production depending on the intensity of the solar radiation, which was monitored by a radiometer. For 0.5_Pt/TiO₂ at the highest irradiance of more than 450 W/m², the H_2 production value was more than twice as high as at the lowest measurement of 205 W/m², where the H_2 production efficiency was 30.61 mmol $H_2/(h \cdot g_{cat})$. The lower efficiency of hydrogen production was due to the lower radiation intensity and the type of reactor construction which was confirmed by the application of an artificial light source (lamps XBO). At the same process parameters under visible light lamp for Pt-modified catalysts (0.5_Pt/TiO₂) 28.53 mmol $H_2/h \cdot g_{cat}$ and 25.17 mmol $H_2/(h \cdot g_{cat})$ were analyzed for 150 W and 100 W, respectively. It was already shown in our previous study (Bednarczyk et al., 2018) that light intensity is a very important factor in photocatalytic H_2 production. It was shown that a decrease in lamp power by as much as 75 W reduces the efficiency of hydrogen generation by about 25% to 30%, depending on the photocatalyst used.

3.4. Mechanism consideration

For experiments performed under natural sunlight irradiation in the gas phase, mainly hydrogen, oxygen, and small amounts of carbon dioxide were detected. During the experiments, the pH of the liquid reaction mixture was measured in addition to the concentration of CO_2 in the gas phase. At the beginning

of the experiments, the pH was $\sim$ 6.4, and after 120 min of irradiation, it decreased to about 3.9. CO_2 concentration measurements showed an increase from 325 to 390 ppm (by weight). The pH of the solution decreased as a result of the dissolution of carbon dioxide in the water. The liquid phase analysis showed that the reduction of glycerol concentration was small, within the error margin of 1–2%. Therefore, it was concluded that glycerol acted mostly as a sacrificial agent (hole scavenger) to enhance photocatalytic hydrogen production rates and enhance the water-splitting reaction. However, based on the liquid phase analysis in which formic acid, acetic acid, diglycerol, and 2-amino-1-1-3-propanodiol have been detected, the conversion of glycerol can be considered as a small part of the mechanism of H_2 generation (Villachica-Llamosas et al., 2024). This suspension is confirmed by the increasing concentration of CO_2 in the gas phase. Only during the photocatalytic production of hydrogen with the addition of glycerin were gaseous products H_2 and CO_2 detected. Although the amount of CO_2 is not much due to the low degree of glycerol conversion, some CO_2 dissolves in water and affects the pH of the solution.

The capture of photogenerated electrons from Pt and Pd photodeposited on TiO_2 represses the recombination of electron-hole pairs and facilitates/accelerates the transfer of holes on the TiO_2 surface. The photocatalytic activity is enhanced in terms of a longer electron-hole pair separation lifetime. The appropriate Fermi level position of Pt or Pd with its high work function initiates an effective Schottky barrier preventing the undesirable migration of electrons back into the conduction band of TiO_2. H_2 may be generated by the reduction of two protons originating from both water and glycerol, the sacrificial agent. And at the same time, glycerol and water in the presence of Pt or Pd photodeposited on TiO_2 and sunlight are converted to H_2 through photocatalytic splitting of water and light-induced oxidation of glycerol. It is known that in

alcohol photoreforming, H_2 production is promoted by the presence of H atoms at the α-position with respect to the hydroxyl group (Villachica-Llamosas et al., 2024).

3.5. Photocatalytic H_2 generation from synthetic and real crude glycerol solution

To investigate organic impurities, influence on the generation of H_2 and oxidation of organic compounds, a preliminary study focused on photocatalytic oxidation was performed. Based on recent studies (Bednarczyk et al., 2018; Gomes et al., 2017; Gmurek et al., 2019) and our experimental results, we concluded that photocatalytic oxidation of various organic wastes, and even toxic organic compounds such as parabens, could be a promising and environmentally friendly method for co-producing hydrogen. The efficiency values obtained for photocatalytic oxidation of 4 hydroxybenzoic acid esters (parabens, methyl (MP), ethyl (EP), and benzylparaben (BeP)) are shown in Fig. 7.
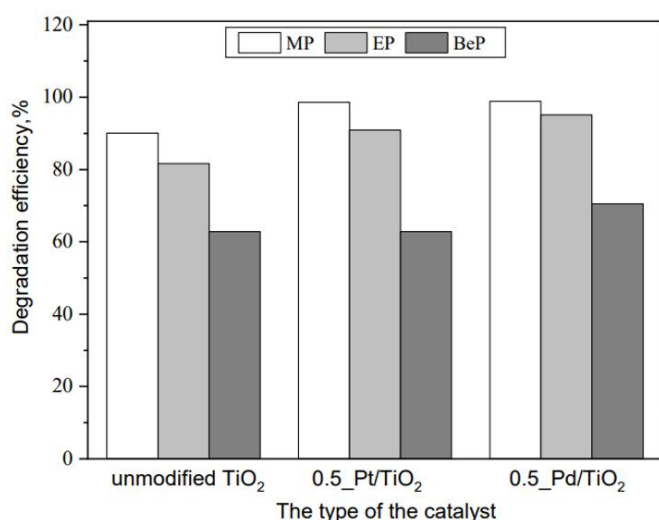
Figure 7. Photodegradation efficiency of different parabens after 120 min for mixtures containing various catalysts (0.07 g/L).

The degradation efficiency of the organics increased when noble-metal-modified photocatalysts were used. The suitability of modified catalysts for both H_2 production and photocatalytic oxidation of organic esters was investigated. Therefore, the viability of both processes occurring simultaneously in solutions of synthetic and real crude glycerol was studied as well. Three experiments with different solutions that mimic synthetic crude glycerol were performed and the results were compared with those obtained for real crude glycerol. The first experiments were carried out with water–glycerol solutions containing only 4.5 wt.% GLC. Second, synthetic crude glycerol containing 1.5 wt.% of GLC, 1 wt.% of MeOH, and 2 wt.% vegetable oil (maintaining the overall concentration of additives at 4.5 wt.%). Third, synthetic crude glycerol was

prepared by adding 0.1 wt.% 4-hydroxybenzoic acid methyl ester (methylparaben, MP) to the second solution. The hydrogen yields of these solutions are shown in Fig. 8. It should be noted that during all experiments no changes in the MP concentration were observed. Hence, it was assumed that photodegradation of MP did not occur because of a lack of oxygen, and hence, limited production of reactive oxygen species. However, the addition of MP significantly increased the efficiency of hydrogen production efficiency; after 60 min, it was more than 50 mmol $H_2/(h \cdot g_{cat})$. Compared to experiments with synthetic crude glycerol, those using 4.5 wt.% real crude glycerol (obtained from the production of biodiesel) showed a much lower H_2 yield of 5.5 mmol $H_2/(h \cdot g_{cat})$, which was attributed to various impurities in the crude glycerol. Contaminants, such as dyes and lubricants, have a negative effect on light dispersion, decreasing the efficacy of the photocatalytic process.
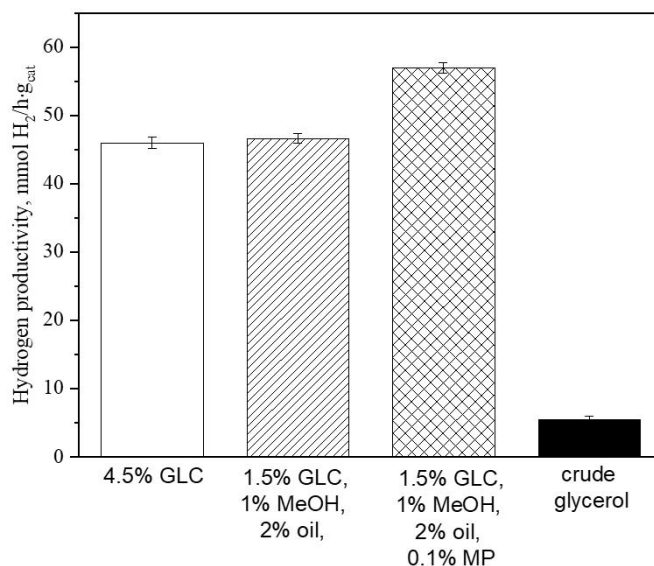
Figure 8. Effect of the addition of methylparaben on hydrogen production with 0.083 g/L of 1 wt.% Pt/TiO_2.

4. CONCLUSIONS

Green hydrogen energy is urgently needed and accelerating the expansion for industrial applicability is essential. This study examined the enlargement of H_2 photocatalytic generation from glycerol solution, transitioning from a small laboratory setup (13 mL) to a larger setup (800 mL). Key aspects included artificial agents, reactor design, cocatalyst type, and dose. The platinum-loaded catalyst showed the highest hydrogen production rate, with an optimal platinum content of 0.5 wt.%. Hydrogen productivity depended on both the metal modification content and the total catalyst concentration. Considering catalyst costs, a concentration of 0.05 g per 600 mL (0.083 g/L) was optimal, producing 5.41 mmol of H_2 compared to 9.67 mmol with a 10 times higher dose (0.58 g).

The study highlighted the importance of radiation type and intensity on H_2 production efficiency. Using natural sunlight for photocatalytic hydrogen production proved viable, with the H_2 evolution rate depending on sunlight intensity and weather conditions. There was no significant difference between Pt and Pd modifications under sunlight. Sacrificial agents like glycerol, methanol, ethanol, 1–propanol, and 1–butanol accelerated H_2 production compared to pure water splitting, with glycerol being superior due to its OH groups.

The study confirmed that adding organic compounds can enhance photocatalytic hydrogen production compared to pure water splitting. Glycerol acted as a sacrificial agent, enhancing water-splitting reactions and H_2 production rates. Moreover, H_2 production from waste glycerol, though around ten times lower than from synthetic solutions, offers a promising approach for utilizing crude glycerol. Impurities in waste glycerol significantly reduced productivity, indicating a need for further research to identify and remove detrimental components in the purification process.

SYMBOLS

MP	methyl
EP	ethyl
BeP	benzylparaben
GLC	glycerol
MeOH	methanol
EtOH	ethanol
1–BuOH	1–butanol
1–PrOH	and 1–propanol
BET	specific surface area calculated based on the Brunauer, Emmet and Teller equation, m^2/g
GC	gas chromatography
λ	wavelength of light, nm

REFERENCES

Bednarczyk K., Stelmachowski M., Gmurek M., 2018. T he influence of process parameters on photocatalytic hydrogen production. *Environ. Prog. Sustainable Energy*, 38, 680–687. DOI: 10.1002/ep.12998.

Borowska E., Gomes J.F., Martins R.C., Quinta-Ferreira R.M., Horn H., Gmurek M., 2019. Solar photocatalytic degradation of sulfamethoxazole by TiO_2 modified with noble metals. *Catalysts*, 9, 500. DOI: 10.3390/catal9060500.

Bowker M., Davies P.R., Al-Mazroai L.S., 2009. Photocatalytic reforming of glycerol over gold and palladium as an alternative fuel source. *Catal. Lett.*, 128, 253–255. DOI: 10.1007/s10562-008-9781-1.

Chen W.-T., Chan A., Sun-Waterhouse D., Llorca J., Idriss H., Waterhouse G.I.N., 2018. Performance comparison of Ni/TiO_2 and Au/TiO_2 photocatalysts for H_2 production in different alcohol-water mixtures. *J. Catal.*, 367, 27–42. DOI: 10.1016/j.jcat.2018.08.015.

Chen W.-T., Dong Y., Yadav P., Aughterson R.D., Sun-Waterhouse D., Waterhouse G.I.N., 2020. Effect of alcohol sacrificial agent on the performance of Cu/TiO_2 photocatalysts for UV-driven hydrogen production. *Appl. Catal., A: Gen.*, 602, 117703. DOI: 10.1016/j.apcata.2020.117703.

Cybula A., Priebe J.B., Pohl M.-M., Sobczak J.W., Schneider M., Zielińska-Jurek A., Brückner A., Zaleska A., 2014. The effect of calcination temperature on structure and photocatalytic properties of Au/Pd nanoparticles supported on TiO_2. *Appl. Catal., B*, 152–153, 202–211. DOI: 10.1016/J.APCATB. 2014.01.042.

Daskalaki V.M., Kondarides D.I., 2009. Efficient production of hydrogen by photo-induced reforming of glycerol at ambient conditions. *Catal. Today*, 144, 75–80. DOI: 10.1016/j.cattod.2008.11.009.

Daskalaki V.M., Panagiotopoulou P., Kondarides D.I., 2011. Production of peroxide species in Pt/TiO_2 suspensions under conditions of photocatalytic water splitting and glycerol photoreforming. *Chem. Eng. J.*, 170, 433–439. DOI: 10.1016/j.cej.2010.11.093.

Dean J.A., 1999. *Lange's Handbook of Chemistry*. 15th ed., McGraw-Hill, New York, 3, 30.

Fan W., Zhang Q., Wang Y., 2013. Semiconductor-based nanocomposites for photocatalytic H_2 production and CO_2 conversion. *Phys. Chem. Chem. Phys.*, 15, 2632–2649. DOI: 10.1039/C2CP43524A.

Fujishima A., Rao T.N., Tryk D.A., 2000. Titanium dioxide photocatalysis. *J. Photochem. Photobiol. C: Photochem. Rev.*, 1, 1–21. DOI: 10.1016/S1389-5567(00)00002-2.

Fujishima A., Zhang X., Tryk D.A., 2007. Heterogeneous photocatalysis: from water photolysis to applications in environmental cleanup. *Int. J. Hydrogen Energy*, 32, 2664–2672. DOI: 10.1016/j.ijhydene.2006.09.009.

Gmurek M., Gomes J.F., Martins R.C., Quinta-Ferreira R.M, 2019. Comparison of radical-driven technologies applied for paraben mixture degradation: mechanism, biodegradability, toxicity and cost assessment. *Environ. Sci. Pollut. Res.*, 26, 37174–37192. DOI: 10.1007/s11356-019-06703-9.

Gomathisankar P., Yamamoto D., Katsumata H., Suzuki T., Kaneco S., 2013. Photocatalytic hydrogen production with aid of simultaneous metal deposition using titanium dioxide from aqueous glucose solution. *Int. J. Hydrogen Energy*, *38*, 5517–5524. DOI: 10.1016/j.ijhydene.2013.03.014.

Gombac V., Sordelli L., Montini T., Delgado J.J., Adamski A., Adami G., Cargnell M., Bernal S., Fornasiero P., 2010. CuO_x–TiO_2 Photocatalysts for H_2 production from ethanol and glycerol solutions. *J. Phys. Chem. A*, 114, 3916–3925. DOI: 10.1021/jp907242q.

Gomes J.F., Bednarczyk K., Gmurek M., Stelmachowski M., Zaleska-Medynska A., Bastos F.C., Quinta-Ferreira M.E., Costa R., Quinta-Ferreira R.M., Martins R.C., 2017. Noble metal–TiO_2 supported catalysts for the catalytic ozonation of parabens mixtures. *Process Saf. Environ.* Prot., 111, 148–159. DOI: 10.1016/j.psep.2017.07.001.

Grabowska E., Marchelek M., Paszkiewicz-Gawron M., Zaleska-Medynska A., 2018. 3 – Metal oxide photocatalysts, In: Zaleska-Medynska A. (Ed.), *Metal oxide-based photocatalysis: Fundamentals and prospects for application. Elsevier*, 51–209. DOI: 10.1016/B978-0-12-811634-0.00003-2.

Greeley J., Jaramillo T.F., Bonde J., Chorkendorff I., Nørskov J.K., 2006. Computational high-throughput screening of electrocatalytic materials for hydrogen evolution. *Nat. Mater.*, 5, 909–913. DOI: 10.1038/nmat1752.

Hainer A.S., Hodgins J.S., Sandre V., Vallieres M., Lanterna A.E., Scaiano J.C., 2018. Photocatalytic hydrogen generation using metal-decorated TiO$_2$: sacrificial donors vs true water splitting. *ACS Energy Lett.*, 3, 542–545. DOI: 10.1021/acsenergylett.8b00152.

Ibhadon A., Fitzpatrick P., 2013. Heterogeneous photocatalysis: Recent advances and applications. *Catalysts*, 3, 189–218. DOI: 10.3390/catal3010189.

Janczarek M., Kowalska E., 2017. On the origin of enhanced photocatalytic activity of copper-modified titania in the oxidative reaction systems. *Catalysts*, 7, 317. DOI: 10.3390/catal7110317.

Jovic V., Chen W.-T., Sun-Waterhouse D., Blackford M.G., Idriss H., Waterhouse G.I.N., 2013. Effect of gold loading and TiO$_2$ support composition on the activity of Au/TiO$_2$ photocatalysts for H$_2$ production from ethanol–water mixtures. *J. Catal.*, 305, 307–317. DOI: 10.1016/j.jcat.2013.05.031.

Kumar D.P., Lakshmana Reddy N., Karthik M., Neppolian B., Madhavan J., Shankar M.V., 2016. Solar light sensitized p-Ag$_2$O/n-TiO$_2$ nanotubes heterojunction photocatalysts for enhanced hydrogen production in aqueous-glycerol solution. *Sol. Energy Mater. Sol. Cells*, 154, 78–87. DOI: 10.1016/j.solmat.2016.04.033.

Kumar D.P., Lakshmana Reddy N., Kumari M.M., Srinivas B., Durga Kumari V., Sreedhar B., Roddatis V., Bondarchuk O., Karthik M., Neppolian B., Shankar V., 2015. Cu$_2$O-sensitized TiO$_2$ nanorods with nanocavities for highly efficient photocatalytic hydrogen production under solar irradiation. *Sol. Energy Mater. Sol. Cells*, 136, 157–166. DOI: 10.1016/j.solmat.2015.01.009.

Lei W., Wang H., Khan S., Suzuki N., Takagi K., Katsumata K.-I., Teshima K., Terashima C., Fujishima A., 2023. Interfacial molecular regulation of TiO$_2$ for enhanced and stable cocatalyst-free photocatalytic hydrogen production. *J. Colloid Interface Sci.*, 645, 219–226. DOI: 10.1016/j.jcis.2023.04.118.

Makula P., Pacia M., Macyk W., 2018. How to correctly determine the band gap energy of modified semiconductor photocatalysts based on UV–Vis spectra. *J. Phys. Chem. Lett.*, 9, 6814–6817. DOI: 10.1021/acs.jpclett.8b02892.

Rafique M., Hajra S., Irshad M., Usman M., Imran M., Assiri M.A., Ashraf W.M., 2023. Hydrogen production using TiO$_2$-Based photocatalysts: a comprehensive review. *ACS Omega*, 8, 25640–25648. DOI: 10.1021/acsomega.3c00963

Sadanandam G., Lalitha K., Kumari V.D., Shankar M.V., Subrahmanyam M., 2013. Cobalt doped TiO$_2$: A stable and efficient photocatalyst for continuous hydrogen production from glycerol: water mixtures under solar light irradiation. *Int. J. Hydrogen Energy*, 38, 9655–9664. DOI: 10.1016/j.ijhydene.2013.05.116.

Stelmachowski M., Marchwicka M., Grabowska E., Diak M., 2014a. The Photocatalytic conversion of (biodiesel derived) glycerol to hydrogen − a short review and preliminary experimental results part 1: a review. *J. Adv. Oxid. Technol.*, 17, 167–178. DOI: 10.1515/jaots-2014-0201.

Stelmachowski M., Marchwicka M., Grabowska E., Diak M., Zaleska A., 2014b. The photocatalytic conversion of (biodiesel derived) glycerol to hydrogen − a short review and preliminary experimental results part 2: photocatalytic conversion of glycerol to hydrogen in batch and semi-batch laboratory reactors. *J. Adv. Oxid. Technol.* 17, 179–186. DOI: 10.1515/jaots-2014-0202.

Villachica-Llamosas J.G., Ruiz-Aguirre A., Colón G., Peral J., Malato S., 2024. CuO−TiO$_2$ pilot-plant system performance for solar photocatalytic hydrogen production. *Int. J. Hydrogen Energy*, 51, 1069–1077. DOI: 10.1016/j.ijhydene.2023.07.149.

Yu J., Hai Y., Jaroniec M., 2011. Photocatalytic hydrogen production over CuO-modified titania. *J. Colloid Interface Sci.*, 357, 223–228. DOI: 10.1016/j.jcis.2011.01.101.

Yu J., Qi L., Jaroniec M., 2010. Hydrogen production by photocatalytic water splitting over Pt/TiO$_2$ nanosheets with exposed (001) facets. *J. Phys. Chem. C*, 114, 13118–13125. DOI: 10.1021/jp104488b.

Zaleska A., 2008. Doped-TiO$_2$: a review. *Recent Pat. Eng.*, 2, 157–164. DOI: 10.2174/187221208786306289.